

INFLUENCE OF THE CALIBRATION POINT IN THE PREDICTION OF THE FRACTURE LOCATION, BASED ON THE LEMAITRE'S DAMAGE MODEL

Raniere S. Neves, raniere_neves@aluno.unb.br

Lucival Malcher, malcher@unb.br

Natália S. I. Aoyama, natalia_seyko@aluno.unb.br

João V. Sahadi, joao_sahadi@aluno.unb.br

UnB – University of Brasília, Faculty UnB Gama, Distrito Federal - Brazil

Filipe X. C. Andrade, filipe.xavier@fe.up.pt

Fábio J. P. Reis, fabio.reis@fe.up.pt

Thiago Doca, thiago.doca@fe.up.pt

IDMEC – Institute of Mechanical Engineering, Faculty of Engineering, University of Porto, Porto, Portugal

***Abstract.** In this paper, it is evaluated the influence of the calibration point in the ability to predict the correct displacement and location to crack initiation, by Lemaitre's damage model. In the first part, a brief review on the theory of the continuum damage mechanics is performance, taking hand the Lemaitre's model with isotropic hardening and isotropic damage. Besides that, an implicit numerical integration algorithm, proposed by De Souza Neto, is implemented in an "in house" academic finite element environment. Then, a calibration of the materials parameters is done, based on an inverse method and a cylindrical smooth bar specimen. At the end, an aluminum alloy 2024-T351 is used and numerical tests are carried out, by cylindrical notched bars with different notches, in order to evaluate the displacement at fracture for different levels of stress triaxiality or loading conditions close and far from the calibration point. The numerical results are compared with experimental data and the level of agreement is evaluated. The ability to predict the correct location to crack initiation is also studied based on the contour of the isotropic damage parameter through the finite element mesh.*

Keywords: damage mechanics, calibration point, fracture location.

1. INTRODUCTION

The fracture in metals is an important subject to be improved, regarding the ability to predict the correct location of crack initiation in machine components and rupture in general structures. This phenomenon can be studied by its separated evolution contribution as the initiation and growth of general micro defects which is induced by large deformations. Some researchers like McClintock (1968) and Rice & Tracey (1969) developed pioneering work undertaken on the subject, where the nature of defect was taken into account the study of ductile damage by analyzing its geometry in a continuous matrix.

The degradation of material properties is an irreversible process and starts from the formation of micro defects which can be voids, cracks and others, that already exist or that will be formed in the material matrix. However, the evolution of material degradation is dependent on macroscopic loading conditions which can cause a volumetric void growth such as in tensile loading condition or a preferential elongation of micro defects which can be observed in pure shear loading conditions. The ductile fracture phenomenon can be described, based on a micromechanical analysis of micro cavity growth, especially for the fracture computation within local approaches of fracture, (see Pineau, 1981; Rousselier, 1987; Besson et al., 2001) or based on the Continuum Damage Mechanics theory and a thermodynamic framework, either phenomenological or micromechanically based, as Lemaitre (1985) for damage caused by plastic flow, Chaboche (1984) and Murakami & Ohno (1981) for creep damage, Krajčinić & Fonseka (1981) on micromechanical grounds.

The formulations proposed by Lemaitre and Gurson are the most important coupled damage ductile models to describe the above two methodologies (see Chaboche et al., 2006). Since then, motivated by the limitations of these classical models, such as in prediction of the correct fracture location or in determination of the correct values of the internal variables at fracture, many researchers have proposed improvements in both methodologies, by introducing more effects in the constitutive formulation or in the damage evolution law like the pressure effect, temperature, Lode angle dependence, viscoplastic effects, crack closure effect, shear mechanisms, among others (Tvergaard & Needleman, 1984; Rousselier, 1980 and 2001; Xue, 2007; Nahshon & Hutchinson, 2008; Lemaitre & Chaboche, 1990; Chaboche, 2003; Andrade Pires et al., 2004; Chaboche et al., 2006; Besson, 2010).

These classical coupled damage models have the ability to predict the correct fracture location under a specific range of stress triaxialities (see Xue, 2007; Nahshon et al.; 2008; Teng, 2008; Malcher, 2011) and are extremely accurate for loading conditions close to the calibration point (see Malcher, 2010). It is useful to take hand of the smooth bar specimen as the calibration point reference and determine the material parameters in this specific loading condition.

Then, when the model is performance for loading conditions far from the calibration point, the numerical results lose accuracy and start to disagree with the experimental evidence (see Malcher, 2010). So, in this paper the dependence of the calibration point is investigated by Lemaitre's model within the range of high level of stress triaxiality.

2. CONSTITUTIVE FORMULATION AND NUMERICAL SOLUTION STRATEGY

2.1. Constitutive formulation

The constitutive equations for ductile damage, described in this section, have been proposed by Lemaitre (1985). Based on the concept of effective stress and the hypothesis of strain equivalence, Lemaitre's model includes the evolution of internal damage, as well as non-linear isotropic and kinematic hardening in the description of the behavior of ductile materials. The constitutive formulation starts from the definition of the Helmholtz specific free energy that can be taken as the state potential of the material and is a function of all state variables. The free energy can be expressed as a function of the set $\{\boldsymbol{\varepsilon}^e, r, D\}$ of state variables:

$$\psi = \psi(\boldsymbol{\varepsilon}^e, r, D) \quad (1)$$

where, ψ represents the specific free energy, $\boldsymbol{\varepsilon}^e$ is the elastic strain tensor, r is the isotropic hardening internal variable and D represents the isotropic damage internal variable.

Under the hypothesis of decoupling between elasticity-damage and plastic hardening, the specific free energy is assumed to be given by the sum:

$$\psi = \psi^{ed}(\boldsymbol{\varepsilon}^e, D) + \psi^p(r) \quad (2)$$

where ψ^{ed} represents the elastic-damage contribution and ψ^p is the plastic contribution to the free energy. The elastic-damage contribution for the free energy can be postulated by the following expression (Lemaitre, 1985):

$$\bar{\rho}\psi^{ed}(\boldsymbol{\varepsilon}^e, D) = \frac{1}{2} \boldsymbol{\varepsilon}^e : (1 - D) \mathbf{D}^e : \boldsymbol{\varepsilon}^e \quad (3)$$

where \mathbf{D}^e represents the isotropic elasticity tensor. The plastic potential can be represented by the isotropic hardening contribution as:

$$\bar{\rho}\psi^p(r) = \bar{\rho}\psi^l(r) \quad (4)$$

The elasticity law is obtained by performing the derivative of the elastic-damage potential (Equation 3) in order to the elastic strain tensor, as:

$$\boldsymbol{\sigma} = \bar{\rho} \frac{\partial \psi^{ed}}{\partial \boldsymbol{\varepsilon}^e} = (1 - D) \mathbf{D}^e : \boldsymbol{\varepsilon}^e \quad (5)$$

The thermodynamical forces conjugated with damage and isotropic hardening internal variable are obtained by performing the derivative of the elastic-damage contribution (Equation 3) in order to the damage variable and by taking the derivative of the plastic potential (Equation 4) in order to the isotropic hardening variable, respectively (Lemaitre *et al.*, 2005):

$$-Y \equiv -\bar{\rho} \frac{\partial \psi^{ed}}{\partial D} = \frac{q^2}{6G \cdot (1 - D)^2} + \frac{p^2}{2K \cdot (1 - D)^2} \quad (6)$$

$$R \equiv -\bar{\rho} \frac{\partial \psi^l}{\partial r} = R(r) \quad (7)$$

where, Y represents the thermodynamic force associated with damage, $q = \sqrt{\frac{3}{2} \mathbf{s} : \mathbf{s}}$ is the von Mises equivalent stress, p is the hydrostatic pressure, G is the shear elasticity modulus, K is the elastic compressibility modulus and R represents the thermodynamic force associated with the isotropic hardening variable.

The evolution of the internal variable can be obtained by assuming the existence of the flow potential, Ψ , given by:

$$\Psi = \Phi + \frac{S}{(1-D) \cdot (s+1)} \cdot \left(\frac{-Y}{S}\right)^{s+1} \quad (8)$$

where, the parameters S and s are damage evolution constants and Φ represents the yield function, which is, defined as:

$$\Phi = \frac{q}{(1-D)} - \sigma_{y_0} - R(r) \quad (9)$$

where σ_{y_0} is the initial uniaxial yield stress. According to the hypothesis of generalized normality, the plastic flow is given by:

$$\dot{\boldsymbol{\varepsilon}}^p = \dot{\gamma} \mathbf{N} \quad (10)$$

$$\mathbf{N} = \sqrt{\frac{3}{2} \frac{\mathbf{S}}{\|\mathbf{S}\|}} \cdot \frac{1}{(1-D)} \quad (11)$$

where $\dot{\gamma}$ is the plastic multiplier, \mathbf{N} represents the flow vector according to Lemaitre's model (1985) and \mathbf{S} is the deviatoric stress tensor. The evolution law for damage and for the isotropic hardening internal variable can be established by performing the derivative of the flow potential (Equation 8) in order to the thermodynamic force associated with damage, Y , and the isotropic hardening variable, r , respectively:

$$\dot{D} \equiv \dot{\gamma} \frac{\partial \Psi}{\partial Y} = \dot{\gamma} \frac{1}{(1-D)} \cdot \left(\frac{-Y}{S}\right)^s \quad (12)$$

$$\dot{r} \equiv \dot{\gamma} \frac{\partial \Psi}{\partial R} = \dot{\gamma} \quad (13)$$

The complementary law of the rate-independent plasticity also needs to be fulfilled:

$$\dot{\gamma} \geq 0, \quad \Phi \leq 0, \quad \dot{\gamma} \Phi = 0. \quad (14)$$

The constitutive equations of Lemaitre's model with isotropic hardening and isotropic damage, employed in this work, are conveniently summarized in Box 1.

Box1. Lemaitre's model with isotropic hardening and isotropic damage.

<p>(i) Elasto-plastic split of the strain tensor: $\boldsymbol{\varepsilon} = \boldsymbol{\varepsilon}^e + \boldsymbol{\varepsilon}^p$</p> <p>(ii) Coupled elastic-damage law: $\boldsymbol{\sigma} = (1-D)\mathbf{D}^e : \boldsymbol{\varepsilon}^e$</p> <p>(iii) Yield function: $\Phi = \frac{q}{(1-D)} - \sigma_{y_0} - R(r)$</p> <p>(iv) Plastic flow and evolution equations for r and D</p> $\dot{\boldsymbol{\varepsilon}}^p = \dot{\gamma} \mathbf{N} = \dot{\gamma} \cdot \sqrt{\frac{3}{2} \frac{\mathbf{S}}{\ \mathbf{S}\ }} \cdot \frac{1}{(1-D)}$ $\dot{r} = \dot{\gamma} \quad \text{and} \quad \dot{D} = \dot{\gamma} \frac{1}{(1-D)} \cdot \left(\frac{-Y}{S}\right)^s$ <p style="text-align: center;">with Y given by: $-Y = \frac{q^2}{6G \cdot (1-D)^2} + \frac{p^2}{2K \cdot (1-D)^2}$</p> <p>(v) Loading/unloading criterion</p> $\dot{\gamma} \geq 0, \quad \Phi \leq 0, \quad \dot{\gamma} \Phi = 0.$
--

2.2. Numerical integration algorithm

Regarding an implicit solution, algorithms based on operator split methodology are especially suitable for the numerical integration of the evolution problem and have been widely used in computational plasticity (see Simo & Hughes, 1998; De Souza Neto et al., 2008). This method, which is used here, consists of splitting the problem in two parts: an elastic predictor, where the problem is assumed to be elastic and, a plastic corrector, in which the system of residual equations comprising the elasticity law, plastic consistency and the rate equations is solved, taking the results of the elastic predictor stage as initial conditions. In the case of the yield condition has been violated, the plastic corrector stage is initiated and the Newton- Raphson procedure is used to solve the discretised equations. The Newton-Raphson procedure was chosen motivated by the quadratic rates of convergence achieved which results in return mapping procedures computationally efficient (see Simo & Hughes, 1998; De Souza Neto et al., 2008). The implicit numerical integration algorithm for Lemaitre's constitutive model was proposed by De Souza Neto (2002) and the overall algorithm for numerical integration is summarized in Box 2.

Box 2. Fully implicit Elastic predictor/Return mapping algorithm for Lemaitre's model.

<p>(i) Evaluate the elastic trial state: Given the incremental strain $\Delta\epsilon$ and the state variables at t_n:</p> $\begin{aligned} \boldsymbol{\epsilon}_{n+1}^{e \text{ trial}} &= \boldsymbol{\epsilon}_n^e + \Delta\boldsymbol{\epsilon} & ; & & R_{n+1}^{\text{trial}} &= R_n & ; & & D_{n+1}^{\text{trial}} &= D_n \\ \tilde{\boldsymbol{S}}_{n+1}^{\text{trial}} &= 2G\boldsymbol{\epsilon}_{n+1}^{e \text{ trial}} & ; & & \tilde{p}_{n+1} &= K\boldsymbol{\epsilon}_{v n+1}^{e \text{ trial}} & ; & & \tilde{q}_{n+1}^{\text{trial}} &= \sqrt{\frac{3}{2}}\ \tilde{\boldsymbol{S}}_{n+1}^{\text{trial}}\ /(1-D_n) \end{aligned}$ <p>(ii) Check plastic admissibility: IF $\Phi^{\text{trial}} = \tilde{q}_{n+1}^{\text{trial}} - \sigma_y^{\text{trial}}(R_{n+1}^{\text{trial}}) \leq 0$ THEN</p> <p style="padding-left: 40px;">set $(\cdot)_{n+1} = (\cdot)_{n+1}^{\text{trial}}$ (<i>elastic step</i>) and go to (v)</p> <p style="padding-left: 40px;"><i>ELSE go to (iii)</i></p> <p>(iii) Return mapping (<i>plastic step</i>): Solve the equation below for $\Delta\gamma$, using Newton-Raphson method.</p> $F(\Delta\gamma) \equiv \omega(\Delta\gamma) - \omega_n + \frac{\Delta\gamma}{\omega(\Delta\gamma)} \left(\frac{-Y(\Delta\gamma)}{S} \right)^s = 0$ <p>where,</p> $\omega(\Delta\gamma) = 1 - D_{n+1} = \frac{3G \cdot \Delta\gamma}{\tilde{q}_{n+1}^{\text{trial}} - \sigma_y(R_n + \Delta\gamma)}$ $-Y(\Delta\gamma) \equiv \frac{[\sigma_y(R_n + \Delta\gamma)]^2}{6G} + \frac{\tilde{p}_{n+1}^2}{2K}$ <p>(iv) Update the others state variables:</p> $R_{n+1} = R_n + \Delta\gamma$ $p_{n+1} = \omega(\Delta\gamma) \tilde{p}_{n+1} \quad ; \quad q_{n+1} = \omega(\Delta\gamma) \sigma_y(R_{n+1})$ $\boldsymbol{S}_{n+1} = \frac{q_{n+1}}{\tilde{q}_{n+1}^{\text{trial}}} \tilde{\boldsymbol{S}}_{n+1}^{\text{trial}} \quad ; \quad \boldsymbol{\sigma}_{n+1} = \boldsymbol{S}_{n+1} + p_{n+1} \boldsymbol{I}$ $\boldsymbol{\epsilon}_{n+1}^e = \frac{1}{2G} \boldsymbol{S}_{n+1} + \frac{1}{3} \boldsymbol{\epsilon}_{v n+1}^{e \text{ trial}} \boldsymbol{I}$ <p>(v) Exit</p>

3. GEOMETRY, MESH DEFINITION AND CALIBRATION PROCEDURE

In the following, the geometry of each specimen, which will be used in the numerical simulation, is presented as well as the mesh definition. Figure 1 shows the dimensions for both cylindrical notched bars, one with a notch radius equal to $R = 4 \text{ mm}$ and other with $R = 12 \text{ mm}$, together with a smooth bar specimen.

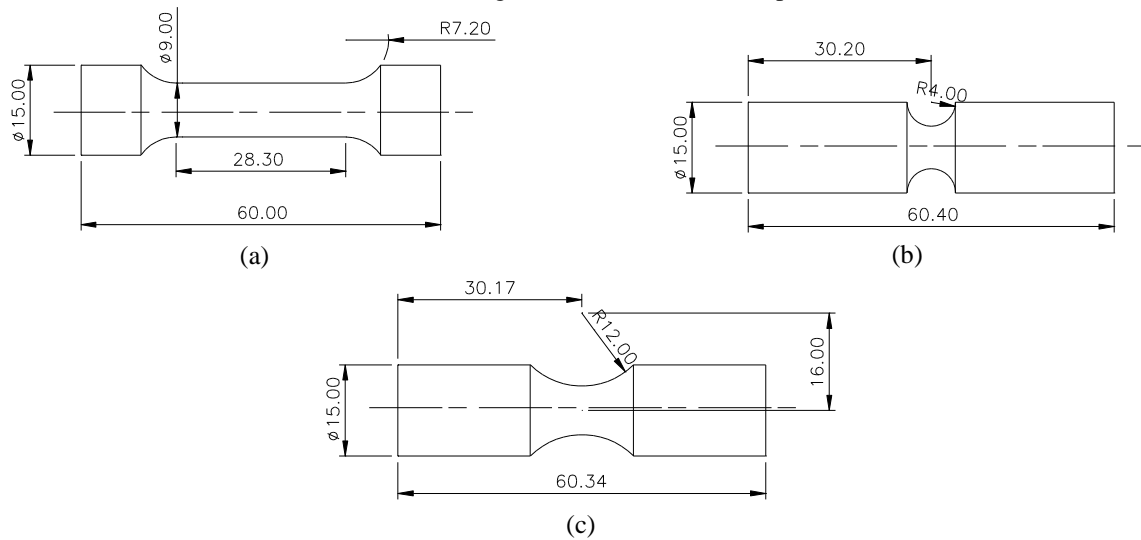


Figure 1. Geometry of the cylindrical notched bars and the smooth bar specimen (dimensions in mm). The specimens were reproduced from Teng (2008).

In order to capture the necking pattern and the evolution of internal variables, a relatively fine discretization is used in the region surrounding the smaller cross-section of the specimens. The standard eight-noded axisymmetric quadrilateral element, with four Gauss integration points, is adopted. The initial mesh discretization for the three cases is illustrated in Figure 2, where only one symmetric quarter of the problem, with the appropriate symmetric boundary conditions imposed to the relevant edges, is modeled.

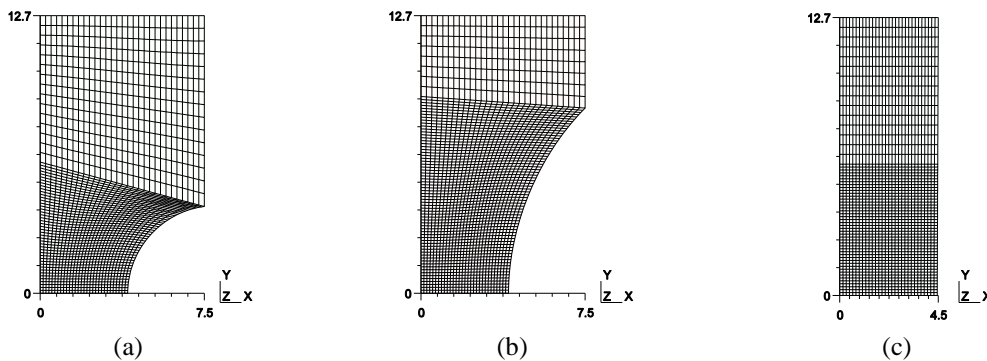


Figure 2. Finite element meshes for the cylindrical notched bar specimens (a) $R = 4 \text{ mm}$, (b) $R = 12 \text{ mm}$ and for the (c) smooth bar specimen.

A total number of 1800 elements has been used in the discretization of both the smooth bar (see Figure 2c) and the notched bar with radii of $R = 4 \text{ mm}$ (see Figure 2a), amounting to a total of 5581 nodes. The mesh of the notched bar with radii of $R = 12 \text{ mm}$ (see Figure 2b) has got 2250 elements and 681 nodes. In all cases, the gauge used is equal to 25.4 mm .

In order to perform the numerical simulations, it is indispensable to obtain the material properties, the stress-strain curve and the damage parameters employed by the Lemaitre's model. An aluminum alloy 2024-T351, which is strongly dependent on both pressure and Lode angle, is used. In this paper, the damage parameters of Lemaitre's model, namely the exponent, s , and denominator, S , of the evolution law, were obtained by Teng (2008) that conducted a study on the numerical prediction of slant fracture with continuum damage mechanics. However, the stress-strain curve and the critical damage values were not taken from the literature but instead numerically determined. Thus, the strategy employed to determine the undamaged stress-strain curve and the critical damage value for the present constitutive damage model, starting from an experimental result for a smooth bar specimen, where having at hand the experimental displacement to fracture ($u_f = 6.65 \text{ mm}$) together with the reaction-displacement, an inverse and iterative methodology was conducted. The objective is to identify the stress-strain curve for each constitutive model such that the force-

displacement curve is as close as possible to the experimental one. Figure 3 shows the reaction curve obtained for Lemaitre’s model after the application of the inverse identification method. It was possible to obtain a close agreement for the constitutive model.

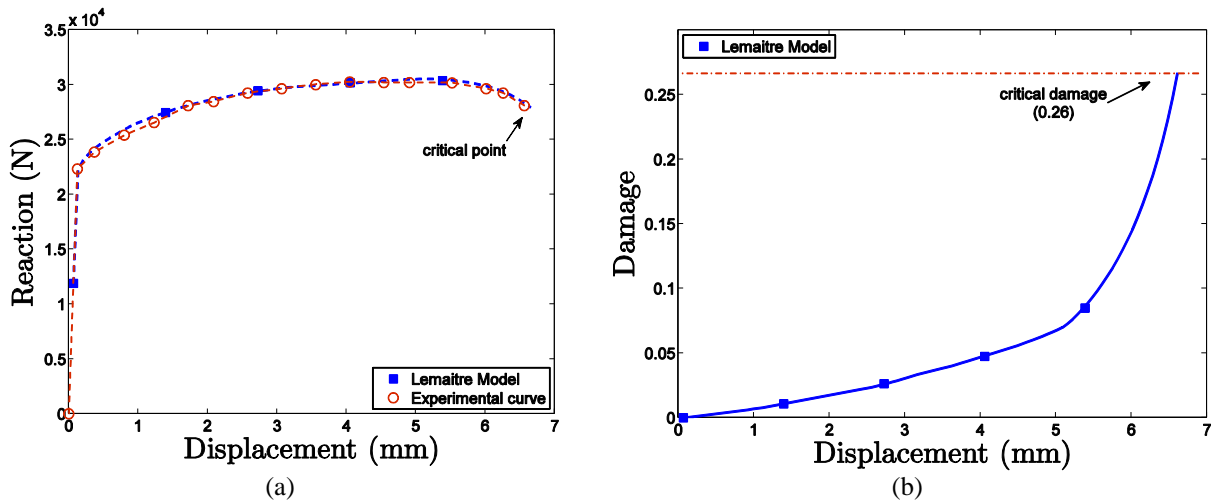


Figure 3. (a) Reaction versus displacement curve for all models and experimental results. (b) Critical damage parameter calibrated for the experimental displacement to fracture ($u_f = 6.65$ mm).

The results of the calibration procedure for the stress-strain curves can be observed in Figure 4. The undamaged stress-strain curve obtained for Lemaitre’s model has got a more pronounced hardening than the von Mises model, which is depicted in Figure 4 and labeled as “uncoupled damage model”, is the curve that includes the effect of damage in the hardening.

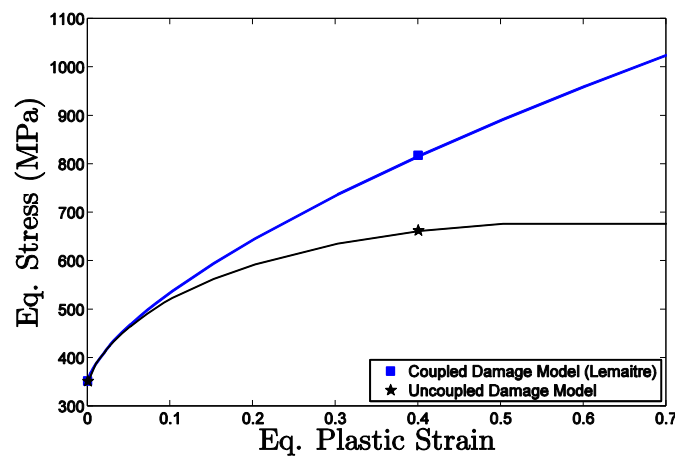


Figure 4. Stress-strain curves for all constitutive models.

The critical value for the damage variable was also obtained from the simulation of the stretching of the smooth bar. All the aforementioned parameters are conveniently listed in Table 1.

Table 1. Material properties for the 2024-T351 aluminum alloy.

Description	Symbol	Value
Elastic Modulus	E	72.400 [MPa]
Poisson’s ratio	ν	0.33
Initial yield stress	σ_{y0}	352 [MPa]
Damage data (exponent)	s	1
Damage data (denominator)	S	6 [MPa]
Critical damage	D_c	0.26

4. NUMERICAL RESULTS

After the calibration procedures of material parameters for the Lemaitre's model, in this part of the paper, numerical simulations are carried out for three different specimens. The numerical displacement at fracture is determined for each specimen under tensile loading condition and compared with experimental data. Figure 5 represents the reaction versus displacement curves determined numerically. It can be observed that when the applied loading condition deviates from the calibration point, the displacement at fracture determined numerically disagree with the displacement experimentally observed. Figure 5a represents the calibration point and both displacements are the same. When the stress triaxiality is increasing (notched bars with notches of $R = 12 \text{ mm}$ and $R = 4 \text{ mm}$), the difference between the two displacements becomes increasingly high, making the model loses accuracy (see Figure 5b and 5c).

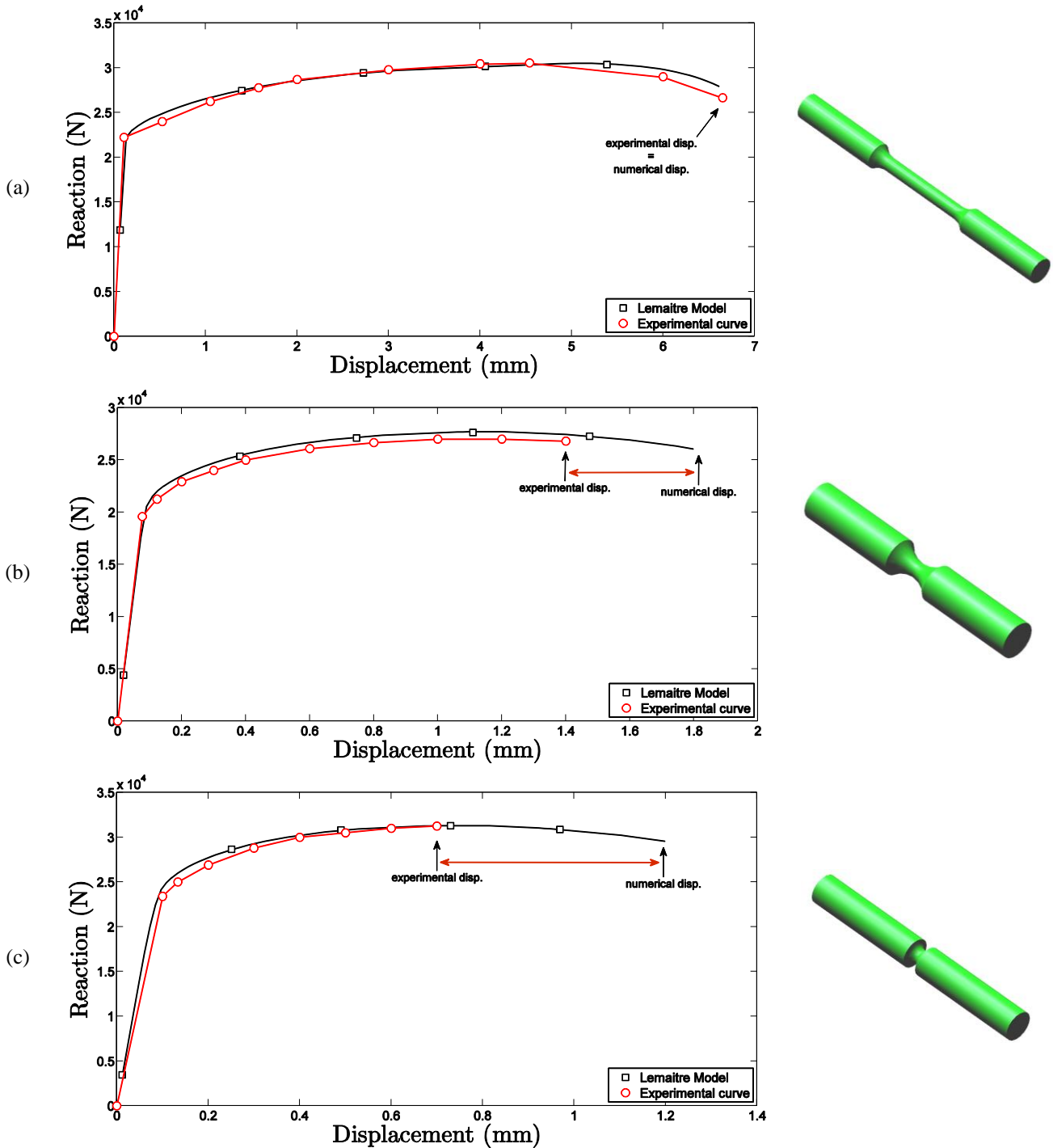


Figure 5. Reaction versus displacement curves. (a) smooth bar specimen, (b) notched bar specimen $R = 12 \text{ mm}$ and (c) notched bar specimen $R = 4 \text{ mm}$.

The numerical and experimental values for the critical displacement can be observed through Table 2.

Table 2: Experimental and numerical displacement at fracture.

Specimen	Stress triaxiality	Experimental displacement (1)	Numerical displacement (2)	Error % (2)-(1)
Smooth bar	0.33	6.65 mm	6.65 mm	0%
Notched bar $R = 12$ mm	0.47	1.40 mm	1.82 mm	23%
Notched bar $R = 4$ mm	0.74	0.70 mm	1.20 mm	41,6%

The evolution of some internal variables can also be analyzed, as the damage parameter and the equivalent plastic strain at fracture. Figure 6 represents the evolution of both parameters at the critical numerical displacement. The level of equivalent plastic strain decreases with the increase of the stress triaxiality, which is in agreement with experimental data. The expected level of the equivalent plastic strain at fracture for the smooth bar, notched bar $R = 12$ mm and notched bar $R = 4$ mm are 0.53, 0.38 and 0.24, respectively. By Figure 6, the numerical values determined by Lemaitre's model are 0.57, 0.49 and 0.39, respectively for the smooth bar, notched bar $R = 12$ mm and notched bar $R = 4$ mm.

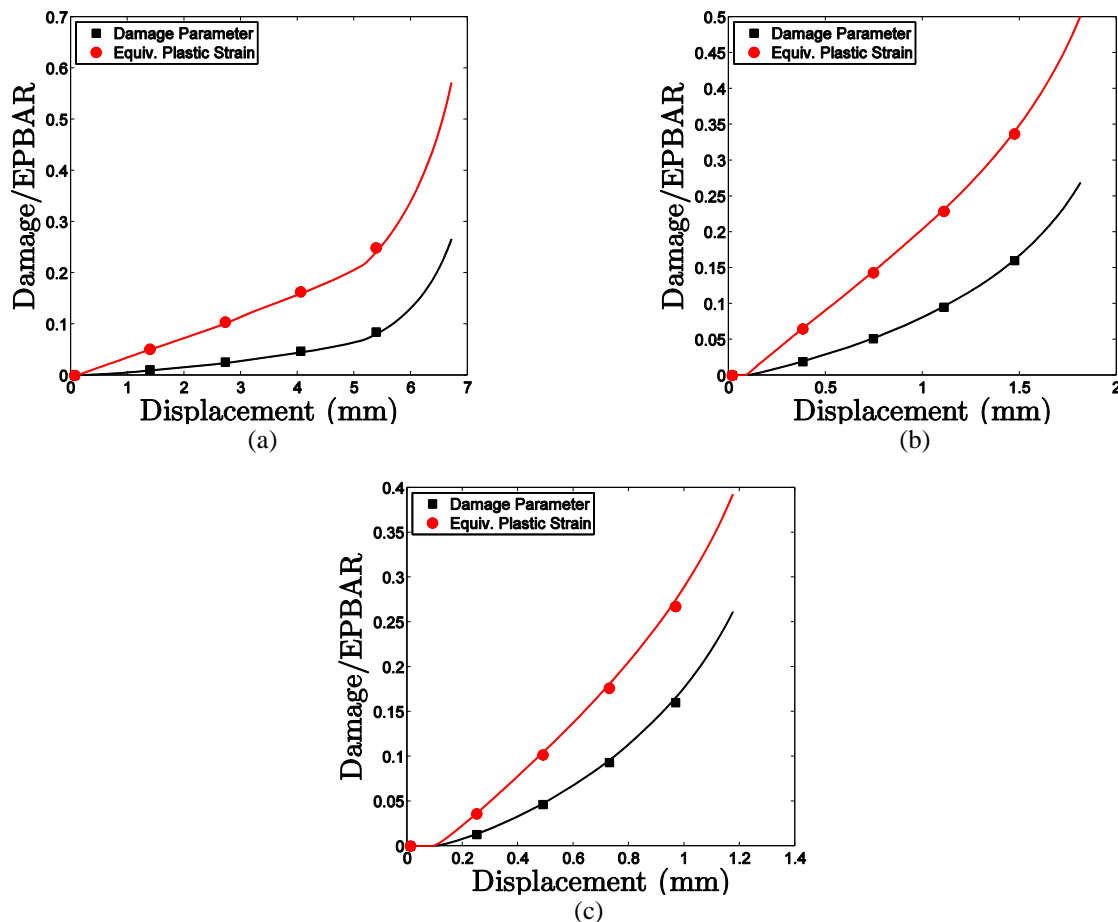


Figure 6. Evolution of damage parameter and equivalent plastic strain at fracture. (a) smooth bar specimen, (b) notched bar specimen $R = 12$ mm and (c) notched bar specimen $R = 4$ mm.

The results can be represented on the space equivalent plastic strain versus stress triaxiality, which is widely called as two dimensional fracture locus (see Figure 7). It can be observed that, in the critical case, the displacement at fracture numerically determined can be 41.6% higher than the experimental data.

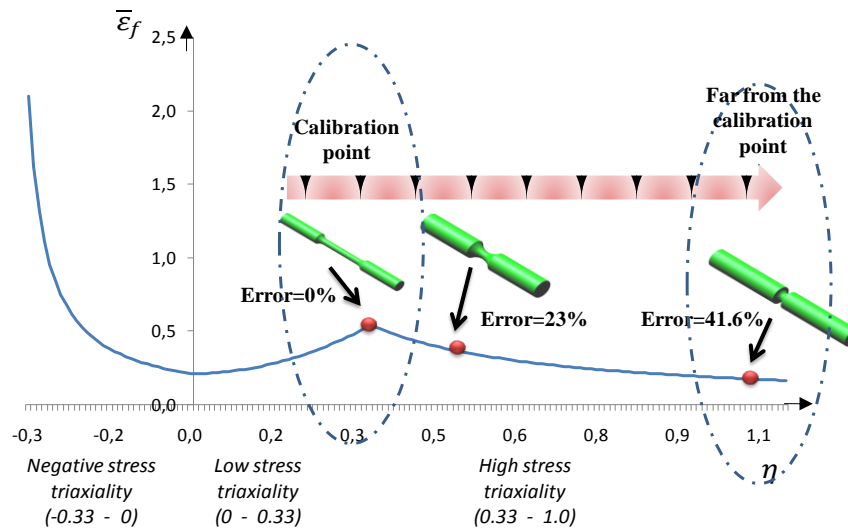


Figure 7. Representation of the error between experimental and numerical displacement for points close and far from the calibration point.

The contour of the damage parameter is represented by Figure 8. According to experimental data (see Teng, 2008), for both specimens, the crack begins in the middle of the specimen and grows to the surface, which was predicted by Lemaitre's model, regarding the location of the maximum value for the damage parameter.

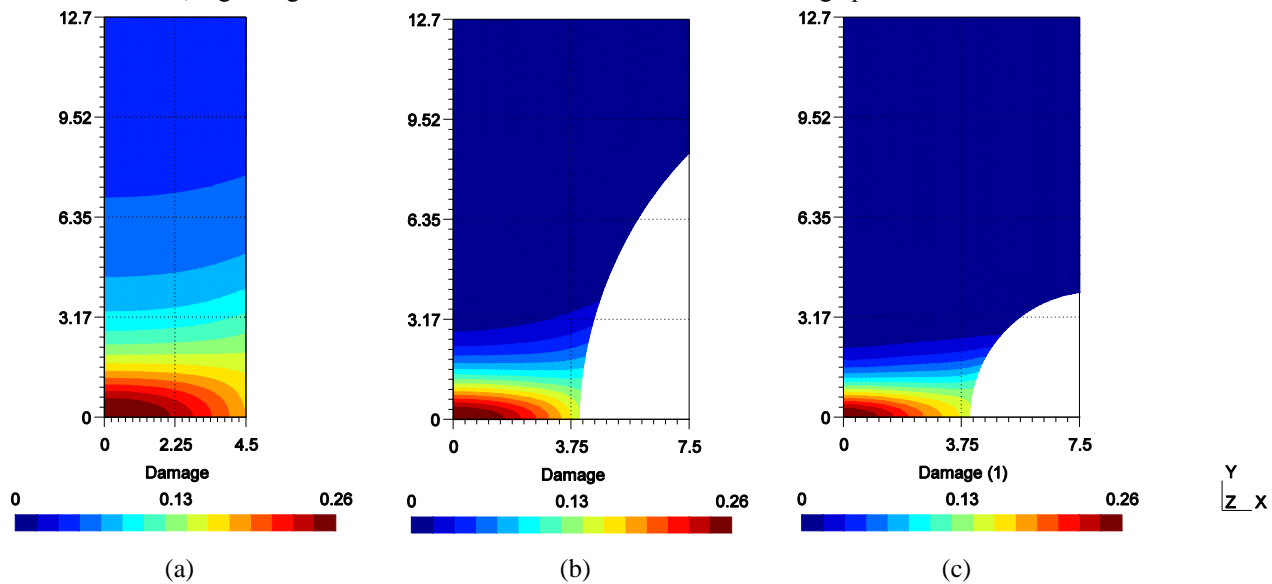


Figure 8. Contour of the damage parameter at the critical numerical displacement. (a) smooth bar specimen, (b) notched bar specimen $R = 12 \text{ mm}$ and (c) notched bar specimen $R = 4 \text{ mm}$.

5. CONCLUSIONS

In this paper, the influence of the calibration point in the accuracy of the numerical results for coupled damage model, as Lemaitre's model, was analyzed. Three different specimens were chosen, regarding the level of stress triaxiality. The materials properties for the aluminum alloy, which is strongly dependent on both pressure and Lode angle, was used. According to comparative analyses between the numerical and experimental displacements at fracture, we can observe that the model is strongly dependent on the calibration point. The numerical displacement at fracture can reach 41% of errors when the loading condition applied is far from the calibration point. By the way, we can conclude and recommend that, for coupled damage models, the loading condition used has to be close to calibration point or the materials parameters requires have to be calibrated for a specifically loading condition that will be used. Even considering the low accuracy in predicting the correct time of fracture onset, in both cases tested, the model could predict the correct location for the potential beginning of fracture.

6. ACKNOWLEDGEMENTS

The authors acknowledge the support of Portuguese Science and Technology Foundation (FCT) and the support of University of Brasília, Faculty UnB at Gama (FGA).

7. REFERENCES

- Andrade Pires, F.M., César de Sá, J.M.A., Costa Sousa, L., Natal Jorge, R.M., 2003, Numerical Modelling of ductile plastic damage in bulk metal forming, *International Journal of Mechanical Sciences*, 45:273–294.
- Besson, J., Steglich, D. and Brocks, W., 2001, Modeling of crack growth in round bars and plane strain specimens. *International Journal of Solids and Structures*, 38(46–47):8259–8284.
- Besson, J., 2010, Continuum Models of Ductile Fracture: A Review. *International Journal of Damage Mechanics*, 19:3–52.
- Chaboche, J.L., 1984, Anisotropic Creep Damage in the Framework of Continuum Damage Mechanics. *Nuclear Engineering and Design*, 79: 309–319.
- Chaboche, J.L., 1987, Continuum Damage Mechanics: Presents State and Future Trends. *Nuclear Engineering and Design*, 105:19–33.
- Chaboche, J.L., 2003, Damage mechanics. In: Milne, I., Ritchie, R.O. and B. Karihaloo (eds.) *Comprehensive Structural Integrity*, vol. 2. Elsevier-Pergamon, pp. 213–284.
- Chaboche, J.L., Boudifa, M., Saanouni, K., 2006, A CDM approach of ductile damage with plastic compressibility. *International Journal of Fracture*, 137:51–75.
- De Souza Neto E.A., 2002, A fast, one-equation integration algorithm for the Lemaitre ductile damage model. *Comm. Num. Meth. Engng.*, 18:541–554.
- De Souza Neto, E.A., Perić, Owen, D.R.J., 2008, *Computational methods for plasticity: theory and applications*. John Wiley & Sons Ltd.
- Krajčinović, D., Fonseka, G.U., 1981, The Continuous Damage Theory of Brittle Materials – Part 1: General Theory. *J. Appl. Mech.*, 48, 809–815.
- Lemaitre, J., 1985, A continuous damage mechanics model for ductile fracture. *Journal of Engineering Materials and Technology - Trans. of the ASME*, 107:83–89.
- Lemaitre, J., Chaboche, J.L., 1990, *Mechanics of Solid Materials*. Cambridge Univ. Press.
- Malcher, L. ; Reis, F.J.P, Andrade Pires, F.M. ; César de Sá, J.M.A ; Andrade, F.X.C., 2010, Numerical tests for shear mechanisms based on two calibration points. In. *CILAMCE 2010 - Mecánica Computacional Vol XXIX*, págs. 2819-2837, Buenos Aires, Argentina.
- Malcher, L. ; Andrade Pires, F.M. ; César de Sá, J.M.A., 2011, An Assessment of Isotropic Constitutive Models for Ductile Fracture under High and Low Stress Triaxiality. *International Journal of Plasticity* - submitted.
- McClintock, F. A., 1971, Plasticity aspects of fracture. In: Leibowitz, H. (Ed.), *Fracture*, vol. 3. Academic Press, pp. 47–225.
- Murakami, S., & Ohno, N., 1981, A Continuum Theory of Creep and Creep Damage. Pages 422–443 of: Ponter, A.R.S. (ed), *Proceedings of the IUTAM Symposium on Creep in Structures*, Leicester, Berlin.
- Nahshon, K., Hutchinson, J., 2008, Modification of the Gurson model for shear failure. *European Journal of Mechanics A/Solids*, 27:1–17.
- Pineau, A., 1981, Review of fracture mechanisms and local approaches to predicting crack resistance in low strength steels. In: François, D. et al. (ed.) *Advances in Fracture Researches*. New-York, Pergamon Press, ICF5. Cannes.
- Rice, J. R., Tracey, D., M., 1969, On the ductile enlargement of voids in triaxial stress fields. *Journal of the Mechanics and Physics of Solids*, 17:201–217.
- Rousselier's, G., 1980, Finite deformation constitutive relations including ductile fracture damage. In: Nemat-Nasser (ed.) *Three-Dimensional Constitutive Relations and Ductile Fracture*. North-Holland Publ. Comp., 1981 pp. 331–355.
- Rousselier's, G., 1987, Ductile fracture models and their potential in local approach of fracture. *Nuclear Engineering and Design* 105: 97–111.
- Rousselier's, G., 2001, The Rousselier model for porous metal plasticity and ductile fracture. In: Lemaitre, J. (ed.) *Handbook of Materials Behavior Models*, vol. 2. Academic Press, New York, chapter 6.6, pp. 436–445.
- Simo, J.C., & Hughes, T.J.R., 1998, *Computational Inelasticity*. New York: Springer-Verlag.
- Teng, X., 2008, Numerical prediction of slant fracture with continuum damage mechanics. *Engineering Fracture Mechanics*, 75:2020–2041.
- Tvergaard, V. and Needleman, A., 1984, Analysis of the cup-cone fracture in a round tensile bar. *Acta Met.* 32:157–169.
- Xue, L., 2007, *Ductile Fracture Modeling – Theory, Experimental Investigation and Numerical Verification*, Ph.D Thesis, Massachusetts Inst. of Technology.